

Cluster size effects in the magnetic properties of $\text{Fe}_p\text{-Al}_{q=1-p}$ alloys

J. B. Santos-Filho¹, A. V. Santos Sá¹, T. S. de Araujo Batista², and J. A. Plascak^{3,4,5}

¹*Instituto Federal de Ciências e Tecnologia de Sergipe 49100-000 São Cristóvão, Sergipe, Brazil*

²*Instituto Federal de Ciências e Tecnologia de Sergipe 49060-108 Aracaju, Sergipe, Brazil*

³*Departamento de Física, Universidade Federal de Minas Gerais,
C. P. 702, 30123-970, Belo Horizonte, MG, Brazil*

⁴*Departamento de Física, Centro de Ciências Exatas e da Natureza, CCEN,
Universidade Federal da Paraíba, Cidade Universitária, 58051-970 João Pessoa, PB - Brazil and*

⁵*Department of Physics and Astronomy, University of Georgia, 30602 Athens GA - USA*

(Dated: December 6, 2019)

A spin-1/2 Ising model, defined in the body centered cubic lattice, is used to describe some of the thermodynamic properties of $\text{Fe}_p\text{-Al}_q$ alloys, with $p + q = 1$. The model assumes, besides the nearest-neighbor exchange coupling, the existence of further next-nearest-neighbor superexchange interactions, where the latter ones depend on the aluminum atoms cluster size. The Ising system so considered is studied by employing Monte Carlo simulations, using a hybrid algorithm consisting of one single-spin Metropolis move together with one single-cluster Wolff algorithm allied, in addition, with single histograms procedures and finite-size scaling techniques. Quite good fits to the experimental results of the ordering critical temperature, as a function of Al concentration in the range $0 \leq q < 0.7$, are obtained and compared to more recent theoretical approaches done on the same alloys.

PACS numbers: 05.10.Ln; 05.70.Fh; 75.10.Hk

Keywords: site-diluted Ising model, Fe-Al alloys, Monte Carlo simulations, phase transition diagram

I. INTRODUCTION

The magnetic and structural properties of iron aluminides have been widely studied for more than a century. This interest is certainly due to their possible industrial application properties such as oxidation and corrosion resistance, good ductility at room temperature, relatively low density, high magnetic permeability value, good vibration damping and insulation properties (for an up to date review of mechanical and some magnetic properties on such compounds see, for instance, reference [1] and references therein). Recent studies have also shown that Fe-Al alloys are promising candidates for data storage, due to the presence of some magnetic patterns appearing at room temperature [2–4]. At the same time, the magnetic properties of Fe-Al alloys are strongly linked to their chemical structure, since depending on composition and synthesis method, they can behave either as a ferromagnet or a paramagnet at room temperature [5–7]. It is also possible to induce in these compounds new types of cooperative phenomena, such as superparamagnetism and reentrant spin glass like phases [8–11]. These characteristics have surely made this alloy one of the most studied binary systems in both experimental and theoretical research points of view.

In particular, the disordered Fe-Al alloys, known as A2 or α -Fe phase, present a lattice structure, with compositional disorder, in the body centered cubic (bcc) lattice [12, 13]. They may be represented by Fe_pAl_q , where p stands for the concentration of iron atoms and q for the concentration of aluminum atoms, with $p + q = 1$. In this way, $q = 0$ corresponds to the pure iron case, which has a ferromagnetic to paramagnetic critical phase transition at a temperature $T_c = 1040$ Kelvin. Due to the fact that

the Al atoms have no magnetic moments, they act indeed as a diluter, and the transition temperature $T_c(q)$ should depend on their concentration q . Nevertheless, the corresponding experimental phase diagram of these alloys in the range of $0 < q < 0.2$ shows a quite small variation of the critical temperature $T_c(q)$ as a function of the concentration q . Such unexpected result is in clear contrast to the theoretical predictions, where a finite negative slope $dT_c(q)/dq|_{q \rightarrow 0} < 0$ is obtained for the transition line [14]. For $0.2 < q < 0.3$, on the other hand, the critical temperature shows a steep slope and eventually vanishes at $q \sim 0.7$.

In order to try to explain this rather anomalous behavior of the phase diagram, several models (including classical and quantum) and theoretical procedures (including analytical approximations and computer simulations), have been proposed in the literature (without any intention of making an extensive review of the previous studies in these alloys, we can cite, for instance, references [15–27]). It should be mentioned that, despite localized spin Hamiltonians are not completely appropriate for the study of these metallic alloys, there are some experimental evidences and first principles calculations making possible the choice of localized models instead of the itinerant ones, as discussed, respectively, in Refs. [15] and [28].

In all the theoretical treatments in the above references, the common ingredient is the assumption that the exchange interaction is dependent on the Al concentration. This is due to the observed expansion of the lattice parameter that is produced when the larger Al atoms replace Fe atoms in the bcc network [15]. The second most common feature present in almost all these approaches is the presence of a superexchange interaction induced

by the Al atoms [16]. This extra ferromagnetic interaction thus links next-nearest-neighbor Fe atoms in the lattice and has also been assumed to depend on Al concentration but be independent of the number of Al atoms that are clustered together. Indeed, with this assumption, a better agreement with the experimental results of the magnetic phase diagram has been obtained. It has been noticed that the results are qualitatively independent whether the model is classical or quantum [17, 20], or even being treated according to some approximation scheme based on mean-field like procedures in the so-called pair approximation. Effective field approaches have also been used to treat the theoretical model [23, 26, 27], as well as Monte Carlo simulations [21]. Although most of the models employed spin-1/2, some spin-1 [24, 27] and spin-2 [26] models have also been considered. In this case, the best results so far for the phase diagram have been achieved by Freitas et al. by using an effective field theory within the one-spin cluster approach [26].

It is worthwhile to mention, however, that the effective field theory in Ref. [26] considers an Ising system with spin-2 and only nearest-neighbor exchange couplings, without any induced superexchange interaction between Fe atoms. In addition, this nearest-neighbor exchange coupling exponentially depends on the Al concentration q . With these assumptions, the best fit to the experimental data has led to an Fe-Fe interaction that increases (of the order of 30%) as the Al concentration increases (up to $q \sim 0.22$), and then decreases to almost zero for $q \sim 1$. This counter-intuitive increase in the Fe-Fe interaction has been recently reported on these compounds, by using first principles calculations, for alloys with rather high Al concentrations, $0.35 \leq q \leq 0.5$, and out of the anomalous region [28]. This increase of the nearest-neighbor exchange coupling with q has been ascribed, in this range of concentrations, to the fact that as the concentration of Al increases, the picture becomes closer to Fe clusters immersed in a sea of Al, with such clusters of now *magnetic* impurities having higher exchange energy and larger moment as compared to greater Fe compositions [28]. However, we do not expect this feature to happen in the anomalous region, since in this region the Al concentration is still small enough to likely behave as a sea for the magnetic atoms. The more plausible role seems indeed to have the Al clusters immersed in a sea of Fe atoms instead. In addition, as will be discussed below, Al clusters of different sizes should behave in different ways.

Another important point concerns the value of the Fe spin. As has been reported in Ref. [28], the spin value of 1/2 seems more appropriate for this system than the value 2 considered in Ref. [26], and even the value 1 in Ref. [24]. Recall still that the fitted crystal field parameter (in units of the ferromagnetic exchange interaction) of the spin-1 Blume-Capel used for these alloys [24] is of the order -10. This rather large negative crystal field means that the probability of occupancy of the zero states of

the spin are quite small, leaving only the ± 1 spin states more probable to occur.

We can now draw our attention to the question of the physical effects of the cluster sizes. One step towards the analysis of the behavior of small clusters of atoms has been achieved from the advent of nanotechnology. It is now known that the elements behave quite differently when their dimensions are reduced to the point of being formed by just a “countable” number of atoms [29]. Recently, researchers have shown, for example, that a cluster of only 102 gold atoms behaves as a giant molecule, instead as of a metal. However, clusters with 144 atoms exhibit in fact a metallic behavior [30]. Since we must visualize the Fe-Al system as being composed of different aluminum clusters dispersed in an iron lattice, we can, by analogy, also assume that the number of Al atoms in a given cluster inside the alloy can, in some way, differently influence the induced superexchange interaction. For instance, only clusters up to a given size are able to switch on the superexchange interaction, while larger clusters are not. This comes to be a reasonable assumption because depending on the superexchange strength, the theoretical slope of the critical temperature as a function of Al concentration turns out to become positive in the limit $q \rightarrow 0$, which is indeed contrary to what has been experimentally observed.

The main goal of this study is exactly to take into account the Al cluster size dependence on the induced superexchange interaction, and treating the regular nearest-neighbor exchange interaction in the same way as done in previous works. For this purpose, we will consider an Ising model and will employ Monte Carlo simulations with a hybrid algorithm consisting of single-spin flip Metropolis and single-Wolff cluster algorithms, together with histograms techniques and finite-size-scaling analysis. Although simulations are, in general, not suitable for fitting experimental results, here we have additionally resorted to a mixed Fortran-Python language subroutines to an easier treatment of the computer simulation data. At the same time, Monte Carlo simulations are in fact very well suited to microscopically study the effects of different Al cluster sizes present in the system for any given aluminum concentration.

The plan of the paper is the following. The model and some details of the simulations are presented in the next section. The results are presented in Section III and some concluding remarks are addressed in the last section.

II. MODEL AND SIMULATIONS

A. Model

As we will assume that aluminum atoms have no magnetic moment, the system under investigation can be well represented by a quenched site-diluted Ising model with Al as dilutors. The Hamiltonian for such spin system can

then be written as

$$\begin{aligned} \mathcal{H} = & - J_1(q) \sum_{\langle nn \rangle} \epsilon_i \epsilon_j S_i S_j \\ & - J_2 \sum_{\langle nnn \rangle} \varsigma_{ij} \epsilon_i \epsilon_j S_i S_j, \end{aligned} \quad (1)$$

where S_i represents an Ising spin-1/2 at the sites of a body centered cubic (bcc) lattice, meaning that we can consider $S_i = \pm 1$. The first sum is over nearest-neighbors (nn) pairs and the second sum over next-nearest-neighbors (nnn) pairs. $J_1(q)$ is the nearest-neighbor interaction given by

$$J_1(q) = J(1 - Aq), \quad (2)$$

where $A > 0$ is an additional theoretical parameter that simulates the decrease of the exchange interaction due to the increase of the lattice parameter as the larger Al atoms concentration q increases. J is the Fe-Fe exchange interaction in the pure undiluted system. The next-nearest-neighbor superexchange interaction J_2 induced by the Al atoms, is given by

$$J_2 = BJ, \quad (3)$$

where the parameter B simply gives the strength of J_2 in units of J . Note that, with the above definition, J_2 is here formally independent on the Al concentration q , contrary as has been assumed in previous works. In Eq. (1), ϵ_i are quenched, uncorrelated random variables, representing the existence of two kinds of particles in the system, namely the magnetic ones (Fe) with $\epsilon_i = 1$, and non-magnetic ones (Al) with $\epsilon_i = 0$. The variable ϵ_i is chosen according to the bimodal probability distribution

$$P(\epsilon_i) = p\delta(\epsilon_i - 1) + q\delta(\epsilon_i). \quad (4)$$

The extra variables ς_{ij} in the second sum of Eq.(1) represent the existence of superexchange interaction between sites i and j . However, this new interaction between iron atoms is now induced only by aluminum atoms on small clusters. The cluster size ζ that induces superexchange interaction between the next-nearest-neighbors is thus another adjustable parameter of the model and is given by just the number of Al atoms, independent of the cluster shape. In this way, $\varsigma_{ij} = 1$ for next-nearest-neighbors i and j adjacent to the border of the cluster, if the cluster size is smaller than ζ , and $\varsigma_{ij} = 0$ otherwise. Fig. 1 depicts a situation where $\zeta = 4$ on a two-dimensional lattice. In Fig. 1(a) the tree Al atom cluster is smaller than $\zeta = 4$, thus being able to generate the next-nearest-neighbor interactions J_2 , while in Fig. 1(b) a cluster of five Al atoms does not induce any J_2 . Of course, all clusters with four spins also induce the superexchange interaction. Note that, with this assumption, although J_2 does not explicitly depend on q , it will be influenced by the Al concentration. The reason is the following. In a quenched dilution, the increase in concentration q leads

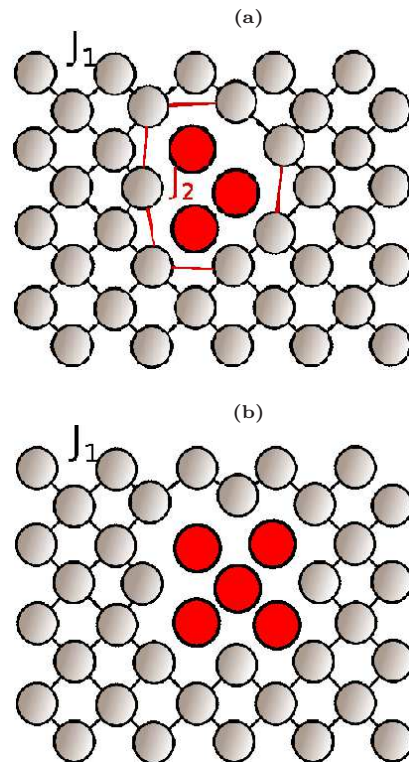


FIG. 1: (Color online) A two-dimensional lattice sketch of the induced superexchange interaction J_2 by the aluminum cluster for $\zeta = 4$. Connected circles are Fe atoms linked by the exchange interaction $J_1 = J_1(q)$, and larger disconnected circles are Al atoms. In (a) the tree Al atoms are able to generate the next-nearest-neighbor interactions J_2 , while in (b) a cluster of five Al atoms does not induce any J_2 .

to the formation of larger Al clusters. Since the probability of finding a cluster with size ζ depends of q , the parameter ζ will indirectly connect the effective number of induced J_2 interaction to the concentration q .

In summary, the present model for these alloys has in fact just three adjustable parameters: parameter A that quantifies the variations of the exchange interaction with the lattice constant; parameter B that quantifies the intensity of the induced superexchange interaction; and parameter ζ that limits the superexchange interaction to small Al cluster. The parameter J is obtained from the critical temperature T_c ($= 1040$ Kelvin) for the pure Fe compound ($q = 0$) or, preferably, one can simply construct the reduced temperature phase diagram by plotting the non-dimensional quantity $T_c(q)/T_c(0)$, as a function of q , in order to easier obtain the fitted parameters.

B. Simulations

The above Hamiltonian has been studied through Monte Carlo simulations. First, we prepare a diluted sample, i.e., for a given value of q , we build a randomly

diluted finite lattice of linear dimension L . Next, we locate and measure all the Al cluster sizes. For all cluster sizes having a number of diluted sites smaller than ζ , the superexchange interaction is switched on between the surrounding next-nearest-neighbor magnetic atoms. Then, we use a hybrid Monte Carlo simulation consisting of one single-spin flip Metropolis algorithm [31, 32], and one single-cluster Wolff algorithm [33]. This hybrid Monte Carlo method [34, 35] has shown to reduce correlations between successive configurations in the simulation. In the present case, one MCS per spin consists of one Metropolis sweep followed by one single-cluster Wolff algorithm (of course different choices of Metropolis and Wolff runs can be implemented, however, the present one turned out to be more efficient if one considers correlations between configurations and the available computer time).

We have computed the magnetization, magnetic susceptibility, and the fourth-order Binder cumulant given, respectively, by

$$m = \frac{1}{N} \sum_{i=1}^N S_i, \quad (5)$$

$$\chi = N \frac{\langle m^2 \rangle - \langle m \rangle^2}{T}, \quad (6)$$

$$U_4 = 1 - \frac{\langle m^4 \rangle}{3\langle m^2 \rangle^2}, \quad (7)$$

where $N = 2L^3$ is the total number of lattice sites. The lattice sizes ranged from $L = 5, 10, 15, 20, 25$ and 30 . The lattice size L and concentration q values have been chosen so that $q \times N$ gives an integer number. All the above values of L have only been used for $q = 0, q = 0.3$ and $q = 0.7$, while for the other points in the phase diagram we have just used $L = 10$ and $L = 20$. It should be stressed that the use of only two lattice sizes can be done, in this case, because the scale of the reduced temperature in the phase diagram does not require a great precision, and also because the error in the simulation results coming from these two lattices alone, when compared to the finite-size extrapolation with larger systems, are smaller than the corresponding symbol sizes used for the experimental and simulational data.

Initially, the simulation runs comprised 1×10^4 MCS per spin for equilibration and the measurements were made over more 1×10^4 MCS at different temperatures, in order to locate the temperature at which the maximum susceptibility occurs or the cumulants cross. Then, a new simulation is performed at this temperature with 3×10^4 MCS per spin for equilibration and new measurements of the corresponding thermodynamic quantities have been made by using single histogram techniques [36, 37] with 1×10^5 additional configurations. For each value of the concentration q , this whole process is repeated by constructing 50 different randomly diluted samples.

III. RESULTS

In Fig. 2 we have typical results of the magnetic susceptibility χ as a function of temperature T , for each of the 50 simulated samples, for concentrations ranging from $q = 0$ to $q = 0.7$ with steps of 0.1, lattice sizes $L = 5, 10, 15$ and 20 , $A = 1.25$, $B = 0.75$, and $\zeta = 60$. The temperature here is measured in units of J/k_B , where k_B is the Boltzmann constant. We have also obtained results for other values of the theoretical parameters A, B and ζ . In Fig. 2 we have chosen the ones that best fit the experimental data. It is clear from this figure that the temperature of the susceptibility peak decreases as the dilution increases, as expected, and above $q = 0.7$ the transition temperature should vanish (the site diluted critical threshold for the bcc lattice is $q_c = 0.7540385(10)$ [38]). We can also observe that the susceptibility peak becomes more dispersed as the concentration of Al atoms increases from $q = 0$ to $q = 0.4$. For example, for $q = 0.1$, in the scale of that figure, the susceptibility curves do not show a sensitive dispersion, and are quite close together. This is a result of the smaller sizes of the Al clusters. On the other hand, for $q = 0.3$ and $q = 0.4$, the peaks show a large variation among the samples, due now to the different cluster sizes present in the random system. As the concentration of Al atoms further increases, there is a kind of saturation of the cluster sizes inside the sample and the dispersion turns out to be again less pronounced.

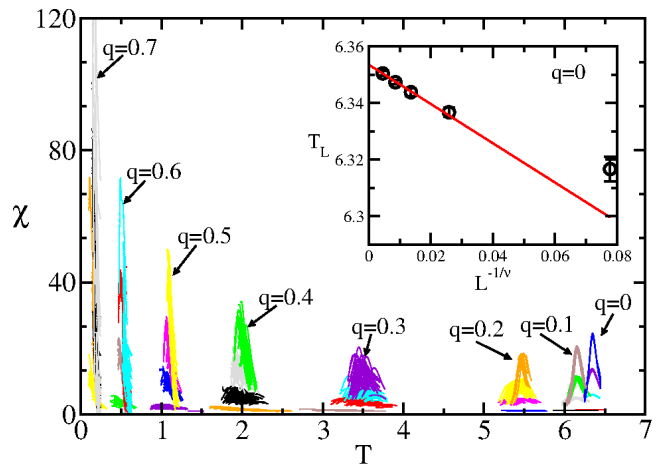


FIG. 2: (color online) Magnetic susceptibility as a function of the temperature for different samples and concentration q values. In this example, for $L = 5$ to $L = 20$; $\zeta = 60$, $A = 1.25$ and $B = 0.75$. For a question of clarity, the individual Monte Carlo data have been omitted and only the lines are shown in this figure. The inset shows the size dependence of the finite-lattice effective critical temperatures estimated from the maximum of χ for $q = 0$, and in this case using $L = 5$ to 30 , with $\nu = 0.6302$ [40]. The value found is $T_c = 6.3535(3)$ without considering the smallest lattice.

The effective transition temperature $T_L(q)$ is thus obtained from the average temperature of each of these

peaks with the standard deviation being the error estimate. As the histogram for each sample has been computed at different temperatures, the estimate of $T_L(q)$ and its error are statistically obtained from 50 different peaks, instead of locating the peak of the averaged susceptibility. The results from both approaches should be, however, equivalent [39]. As an example, the inset in Fig.2 shows the size dependence of the effective critical temperatures for $q = 0$ and $L = 5$ to 30 with the critical exponent $\nu = 0.6302(4)$ taken from the Ref. [40]. The thermodynamic limit extrapolated value for the critical temperature is obtained from

$$T_L = T_c + aL^{-1/\nu}, \quad (8)$$

where a is a non-universal constant. From above equation we obtain $T_c = 6.3535(3)$, where the smallest lattice has not been considered.

Obtaining T_c using the susceptibility maximum and the above equation requires, of course, the knowledge of the critical exponent ν . From universality arguments one knows that this exponent is indeed dependent on the concentration [41]. However, another possibility to find T_c is to use the finite-size scaling of the Binder cumulant, which for large enough lattices is independent of any exponent. We can then follow the variation of U_4 with T for various system sizes and then locate the intersection of these curves for each sample, and finally calculating the mean and standard deviation of all intersections points. Fig. 3 depicts the results for $q = 0$ (in this case we do not have dilution, only different MC runs. The results for other values of q are rather similar, with a larger dispersion as we increase q as noticed in the susceptibility behavior). All the 50 samples results are shown, for each lattice, in a narrow range of temperatures.

The data have been obtained from histograms at different temperatures for each sample. We also opted here to compare the crossings of U_4 for two different lattice sizes L and L' of each sample. The statistics is now obtained from 50×50 data. It is also clear from Fig. 3 that due to the presence of residual corrections to finite size scaling, one still needs to extrapolate the results by doing the limit $1/\ln(L/L') \rightarrow 0$, as has been discussed in Ref. [42]. This procedure is shown in the inset of Fig. 3 for $L' = 10$. From there we obtain $T_c = 6.3542(2)$. This critical temperature for $q = 0$ agrees very well with the previous one obtained from the susceptibility, and also with the high-temperature series expansion estimate by Butera and Comi $T_c = 6.35435(3)$ [40] and with other Monte Carlo results $T_c = 6.35441(5)$ [43], and $T_c = 6.3544(6)$ [25]. This is a quite nice numerical way for us to test the implementations that have been done in the computer codes.

In what follows, the transition temperature has been estimated using this process of cumulant crossings to avoid any use of critical exponents. In addition, we have resorted to Java and Python programming language with the use of some public libraries with NumPy and SciPy [44]. It was then possible to link FORTRAN processing

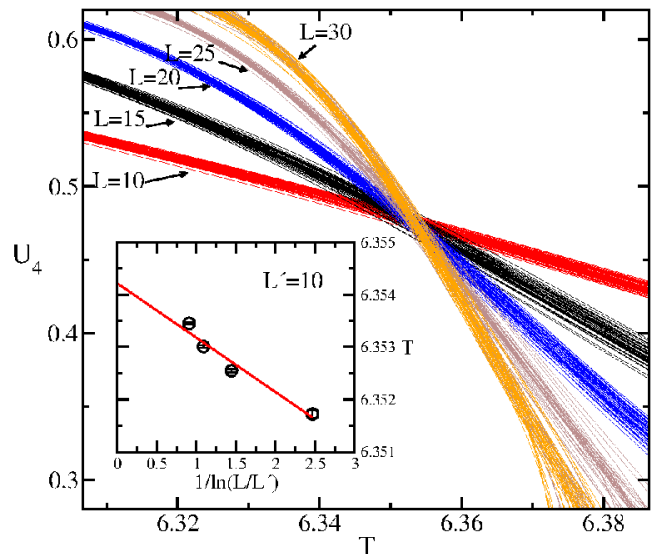


FIG. 3: (Color online) Fourth-order Binder cumulant U_4 as a function of temperature T , for $q = 0$ and 50 random samples for each lattice size ranging from $L = 10$ to $L = 30$. The inset in the figure shows T_L plotted versus the inverse of the logarithm of the scale factor L/L' . The full line is the corresponding linear fit. The estimated temperature is $T_c = 6.3542(2)$.

speed and automate the generation of the phase diagram in a simpler and more parallel way. This made possible to find a good adjustment of the experimental data, even using the present extensive MC simulations. A good adjustment was then obtained with the parameters $\zeta = 60$, $A = 1.25$ and $B = 0.75$.

Before discussing the phase diagram itself, it is illustrative to see the effect of the size of the clusters inducing the superexchange interaction. For this purpose, we have in Fig. 4 the reduced transition temperature $T_c(q)/T_c(0)$ as a function of q , for $A = 1.25$, $B = 0.75$ and different ζ values, for the lattice size $L = 10$ (it is also included in this figure, as a matter of comparison, experimental data from references [45] and [46]). We can observe from this figure that the behavior of the phase diagram is indeed strongly dependent on the cluster size parameter. When $\zeta = 0$, which represents the absence of superexchange interaction, a good fit is only observed for $q > 0.45$, with a finite and negative slope at $q = 0$, contrary to experimental data. On the other hand, for $\zeta = 2L^3$ we have that the superexchange interaction is present in all Al cluster sizes, and a good fit is now obtained only for $q < 0.2$. However, for ζ in range of 10 to 100, not only are the curves close together but also give a better fit to the whole experimental range of concentrations. A more detailed analysis of the data show that $\zeta = 60$ provides the best fit.

Fig. 5 exhibits the transition temperature T_c , now given in Kelvin units, as a function of Al concentration q for the best fit with $A = 1.25$, $B = 0.75$ and $\zeta = 60$, in comparison with the experimental data [45, 46].

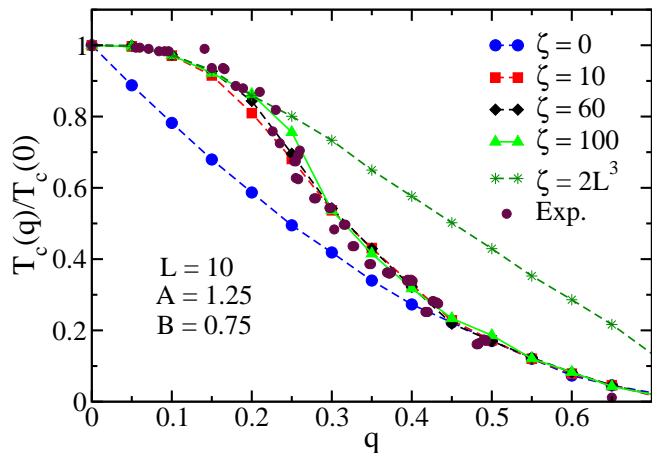


FIG. 4: (Color online) Phase diagram in the reduced temperature $T_c(q)/T_c(0)$ versus concentration q plane for different values of the cluster size ζ for the lattice size $L = 10$. As a matter of comparison, the experimental data coming from several references are also shown. The error bars are smaller than the symbol sizes and the lines are just a guide to the eyes.

The Monte Carlo results have been obtained from finite-scaling extrapolation with $L = 10, 15, 20, 25,$ and 30 for $q = 0, 0.3$ and 0.7 , while for the other concentrations only the cumulant crossings with $L = 10$ and $L = 20$ have been considered. It is also shown in that figure the theoretical fit obtained by Freitas et al. using an effective field approach [26] and Monte Carlo results by Ghosh et al. Ref. [28]. One can clearly see that, apart from the tail for $q > 0.5$, the present results are indeed in better agreement than those from effective field theory [26]. In order to have a more quantitative comparison between both fits, we have also calculated the root mean square error (RMSE), the coefficient of determination, that is the square of the Pearson's product-moment correlation coefficient (r^2), and Willmott index (d) [47]. Since there are fewer simulation points than experimental data, we have calculate a spline univariate interpolation [48] of the simulation data using python's SciPy library [44]. The interpolation is shown by the dashed line in Fig. 5. The obtained results are summarized in Table I. The lower the RMSE value and the closer to 1 are r^2 and d , the closer the model is to the experimental data (see, for instance, Ref. [49] and references therein). In this case, we observe the results obtained with the model proposed in this work is better than the model used by Freitas et al. [26]. We did not make any finer comparison to the results by Ghosh et al. [28] because they only studied one narrow region of the phase diagram and, at the same time, it is visually clear that the present transition curve is definitively closer to the experimental data than the results from [28].

Besides the better agreement of the present approach over the model without any induced next-nearest-neighbor interactions of ref. [26], we can also notice the

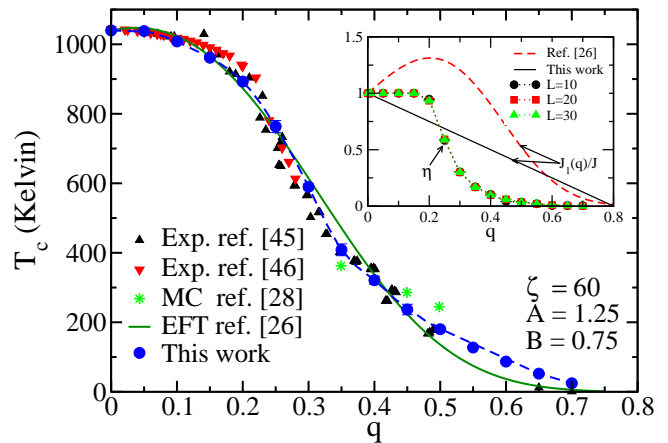


FIG. 5: (Color online) Phase diagram with the temperature T_c , now in Kelvin, as a function of Al concentration q for our best fit parameters. Triangle up and triangle down are, respectively, from references [45] and [46]. Stars come from MC simulations of reference [28] only in the concentration range $0.35 < q < 0.5$. The solid line is the theoretical fit using the effective field theory from reference [26]. Solid circles are the present Monte Carlo simulation results, where the dashed line is their spline univariate interpolation. The inset shows the behavior of the reduced nearest-neighbor interaction $J_1(q)/J$ as a function of q according to Ref. [26] (dashed line) and the present results (full line). It is also shown, in this inset, the Monte Carlo results of the ratio η , defined in Eq. (9), for the largest lattices. In this case, the dotted lines are just guide to the eyes and the error bars are smaller than the symbol sizes.

TABLE I: The root mean square error (RMSE), the coefficient of determination (r^2), and Willmott index (d) obtained in this work and those calculated from the results of Ref. [26].

	This work	Ref. [26]
RMSE	3.5282	4.3275
r^2	0.9949	0.9924
d	0.9972	0.9959

rather strange behavior that the nearest-neighbor interaction must have, as a function of the Al concentration q , when no extra couplings are considered in the theoretical model. This is shown in the inset of Fig. 5. In this case, in order to keep the transition temperature almost constant with dilution, without the presence of a superexchange interaction, the nearest-neighbor coupling $J_1(q)$ has to increase as q increases, in order to balance the broken bonds caused by the diluted atoms. And it indeed increases about 30% for concentrations up to $q \sim 0.22$. However, in view of the calculations from first principles [28] this is not expected, at least in this small range of Al concentrations. This means that a model that takes into account the influence of the size of Al clusters inducing extra interactions in these alloys should be more appropriate to a direct connection to the thermodynamics of the magnetic properties of Fe-Al compounds.

Concerning the adjustments of the theoretical param-

eters A , B and ζ , one should mention that, apart from ζ , which has been obtained in a process depicted in Fig. 4, the first two of them can in fact be roughly estimated, since they affect different regions of the phase diagram, making it easier to fit the critical transition line. For instance, it is noticed that the parameter B mostly influences the initial anomalous region of the diagram ($q < 0.2$). In this region, the Al atoms are more likely to be isolated from each other, so each one breaks 8 nearest-neighbor exchange interactions J_1 and, at the same time, can induce up to most 12 new superexchange interactions J_2 . In order for the dilution effect, in this initial region of the phase diagram, be as minimal as possible, the value of B should be at least $2/3$, keeping in this way the balance of the ferromagnetic interactions. However, as clusters with more than one Al atom can indeed be formed in the alloys, together with the fact that the nearest-neighbor interaction decreases with Al concentration, the best value for the fits should be a little higher, and in the present case it is found $B = 0.75$. On the other hand, the A parameter is mainly used for fits of the diagram in the higher Al concentration range. Its value has been chosen so that there is no antiferromagnetic nearest-neighbor interactions, since neutron scattering data for $q > 0.25$ showed no indication of any antiferromagnetic order [50]. This means that $J_1(q)$ must be positive for concentrations up to $q \sim 0.8$, which is just above the critical value $q_c = 0.7540385(10)$. So, the choice $A = 1.25$. A similar idea has been already used in a previous three-dimensional diluted ferromagnetic XY model [51] to adjust the experimental data of the insulating pentacoordinate iron(III) molecular ferromagnet $\text{Fe}[\text{DSC}]_2\text{Cl}$.

Finally, the present numerical values for the theoretical parameters are comparable to the previous ones using analytical approaches, at least concerning the nearest-neighbor interaction $J_1(q)$. For instance, as the Boltzmann constant $k_B = 8.617 \times 10^5$ eV/K and the experimental result of the critical temperature of the pure Fe system is $T_c = 1040$ K, we obtain $J = 0.014$ eV, a value that is in fully agreement with $J = 0.013$ eV from reference [16] and $J = 0.014$ eV from reference [23]. This agreement comes from the fact that the transition temperature coming from the employed approximations in those works are comparable to the present Monte Carlo result for the bcc lattice. The value of $A = 1.25$ is also comparable to $A = 0.85$ and $A = 0.95$ obtained, respectively, in references [16] and [23]. Notice also that even $\zeta = 60$ is of the order of the size of the gold clusters (~ 100) with molecular-metal behavior [30].

The situation is, however, different concerning the superexchange interaction. In the previous works J_2 , assumed to depend on the concentration q , has a kind of oscillatory behavior, becoming still negative for some range of q , which is not expected for this system. In the present approach, J_2 does not depend on Al concentration, but is instead influenced by the number of clusters that can induce the superexchange interactions. This can be better

seen by tracking the quantity

$$\eta = \frac{N_s}{N_t}, \quad (9)$$

where N_s is the average effective number of superexchange interactions induced by clusters smaller than ζ and N_t is the average of the total number of next-nearest-neighbor Fe atoms surrounding all clusters of the sample. The corresponding behavior of η for the fitted parameter $\zeta = 60$ is also depicted in the inset of Fig. 5. One can clearly see that for low values of the concentrations one has $N_s \sim N_t$, due to the fact that here larger clusters are seldomly formed. But, as the concentration increases, larger clusters are formed and accordingly decreasing the number of superexchange interactions.

IV. CONCLUDING REMARKS

We have used a site diluted spin-1/2 Ising model, with nearest- and next-nearest-neighbor interactions, to describe the magnetic phase diagram of Fe-Al alloys in the bcc lattice. We have employed Monte Carlo simulations based on a hybrid algorithm consisting of one single-spin Metropolis move and one single-cluster Wolff algorithm. In some regions of the phase diagram we have also used single histogram techniques allied with finite-size scaling arguments. With the assumption that only aluminum present in clusters composed of less than 60 Al atoms induce a superexchange interaction among next-nearest-neighbor Fe atoms surrounding the cluster, a good description of the phase diagram could be obtained, including the anomalous region for small Al concentrations.

We have used here Monte Carlo simulations because it seems to be the most suitable approach to properly take into account the Al cluster size effects. Such cluster size properties have not been considered previously and better fits than those from Refs. [15–27] have been achieved. In addition, Monte Carlo simulations provide not only more precise values for the transition temperatures, but also can capture the real physics of the cluster size properties. For this reason, we believe that the fitted theoretical parameters should also be more accurate. In addition, the behavior of the exchange and superexchange interactions with the Al concentration is physically more plausible than those earlier reported for these alloys.

We have not estimated the errors of the fitting parameters in the usual way. We have, however, done some extra simulations just to test the order of sensitiveness the fits exhibit by changing the values of them. For example, the quality of the fit has no significant changes by considering $\zeta = 55$ or 60 , $A = 0.7$ or 0.8 and $B = 1.3$ or 1.2 .

As a final remark, we have not considered the possibility of having a nearest-neighbor exchange interaction that increases as q increases, as pointed out recently in reference [28] for $0.35 < q < 0.5$. We believe that such

oscillatory behavior will not produce significant changes either in the anomalous region or even out of it. In fact, the corresponding Monte Carlo results shown by the stars in Fig. 5 do not exhibit a good agreement neither with the experimental data nor with the theoretical model predictions.

Acknowledgments

The authors would like to thank A. S. Freitas for the availability of the theoretical data obtained using the ef-

fective field theory and M. F. Cavalcante for fruitful discussions. Financial support from the Brazilian agencies CNPq and FAPEMIG are also gratefully acknowledged.

-
- [1] M. Palm, F. Stein and G. Dehm *Annu. Rev. Mater. Res.* **49** (2019).
- [2] J. Sort, A. Concustell, E. Menéndez, S. Suriñach, K. V. Rao, S. C. Deevi, M. D. Baró, J. Nogués, *Adv. Mater.* **18** 1717 (2006).
- [3] E. Menéndez, M. O. Liedke, J. Fassbender, T. Gemming, A. Weber, L. J. Heyderman, K. V. Rao, S. C. Deevi, S. Suriñach, M. D. Baró, J. Sort and J. Nogués, *small* **5**(2) 229-234 (2009).
- [4] R. Bali, S. Wintz, F. Meutzner, R. Hübner, R. Boucher, A.A. Únal, S. Valencia, A. Neudert, K. Potzger, J. Bauch, F. Kronast, S. Facsko, J. Lindner, J. Fassbender, *Nano Lett.* **14** 435 (2014).
- [5] M. J. Besnus, A. Herr, and A. J. P. Meyer, *J. Phys. F* **5** 2138 (1975).
- [6] A. Oubelkacem, I. Essaoudi, A. Ainane, F. Dujardin, J. Ricardo de Sousa, and M. Saber, *Phys. A* **389** 3427 (2010).
- [7] H. B. Rodríguez, D. O. Lozano, Y. A. R. Martínez, J. S. T. Hernández and G. P. Alcazar, *J. Supercond. Nov. Magn.* **29**(5) 1357-1362 (2016).
- [8] A. Arrott and H. Sato *Phys. Rev.* **114**(6) 1420 (1959).
- [9] R. D. Shull, H. Okamoto, and P. A. Beck, *Solid State Commun.* **20** 863-868 (1976).
- [10] P. Böni, S. M. Shapiro, and K. Motoya, *Solid State Commun.* **60** 881-884 (1986).
- [11] S. Takahashi, X. G. Li, and A. Chiba, *J. Phys. Condens. Matter* **8**(50) 11243 (1996).
- [12] L. E. Zamora, G. A. Pérez Alcázar, G. Y. Vélez, J. D. Betancur, J. F. Marco, J. J. Romero, A. Martínez, F. J. Palomares, J. M. González, *Phys. Rev. B* **79** 094418 (2009).
- [13] M. Trautvetter, U. Wiedwald, H. Paul, A. Minkow, P. Ziemann, *Appl. Phys. A: Mater. Sci. Process* **102** (3) 725 (2011).
- [14] R. B. Stinchcombe, in: C. Domb, J.L. Lebowitz (Eds.), *Phase Transitions and Critical Phenomena*, vol. 7, Academic Press, New York, (1983).
- [15] G. A. Pérez Alcázar, J. A. Plascak, and E. Galvão da Silva, *Phys. Rev. B* **34** 1940 (1986).
- [16] J. A. Plascak, L. E. Zamora, G. P. Alcázar, *Phys. Rev. B* **61**(5) 3188 (2000).
- [17] M. Salazar, L. E. Zamora, G. A. P. Alcázar, et al. *Physica B* **320** 236 (2002).
- [18] K. Mota, J. R. de Sousa, C. E. Cordeiro, *J. Magn. Magn. Mater.* **257**107 (2003).
- [19] A. Osorio, W. R. A. Contreras, L. E. Zamora, et al. *Phys. Rev. B* **68** 024420 (2003).
- [20] W. A. Contreras, L. E. Zamora, G. P. Alcázar and J. A. Plascak, *Phys. Rev. B* **72**(5) 052402 (2005).
- [21] W. R. Aguirre-Contreras, L. E. Zamora, G. A. P. Alcázar, et al. *Phys. Lett. A* **360** 411 (2007).
- [22] D. P. Lara, G. A. P. Alcázar, L. E. Zamora, et al. *Phys. Rev. B* **80** 014427 (2009).
- [23] D. A. Dias, J. R. de Sousa, J. A. Plascak, *Phys. Lett. A* **373** 3513 (2009).
- [24] D. A. Dias and J. A. Plascak, *Phys. Lett. A* **375** 2089 (2011).
- [25] I. J. L. Diaz and N. S. Branco, *Phys. Rev. E* **85**(2) 021142 (2012).
- [26] A. S. Freitas, D. F. de Albuquerque, I. P. Fittipaldi, N. O. Moreno *J. Appl. Phys.* **113**(9) 093903 (2013).
- [27] A. S. Freitas, D. F. de Albuquerque, I. P. Fittipaldi and N. O. Moreno *J. Magn. Magn. Mater.* **362** 226 (2014).
- [28] T. Ghosh, A. P. Jena and A. Mookerjee, *J. Alloys Comp.* **639** 583-587 (2015).
- [29] C. C. Koch, *Nanostructured materials: processing, properties and applications*. William Andrew, (2006).
- [30] S. Mustalahti, P. Myllyperkiö, S. Malola, T. Lahtinen, K. Salorinne, J. Koivisto, M. Pettersson, *ACS nano* **9**(3) 2328-2335 (2015).
- [31] N. Metropolis, A.W. Rosenbluth, M.N. Rosenbluth, A.H. Teller, and E. Teller, *J. Chem. Phys.* **21** 1087 (1953).
- [32] M. E. J. Newman, G. T. Barkema, *Monte Carlo methods in statistical physics*, Oxford University Press, USA (1999).
- [33] U. Wolff, *Phys. Rev. Lett.* **62** 361 (1989).
- [34] M. Creutz, *Phys. Rev. D* **36** 515 (1987).
- [35] S. G. Pawig, K. Pinn, *Int. J. Mod. Phys. C* **9** 727 (1998).
- [36] A. M. Ferrenberg and R. H. Swendsen, *Phys. Rev. Lett.* **61**(23) 2635 (1988).
- [37] A. M Ferrenberg and D. P. Landau, *Phys. Rev. B* **44**(10) 5081 (1991).
- [38] C. D. Lorenz and R. M. Ziff, *J. Phys. A* **31** 8147 (1998).
- [39] D. Ivaneyko, B. Berche, Yu. Holovatch, J. Ilnytskyi, *Physica A* **387** 4497 (2008).
- [40] P. Butera and M. Comi, *Phys. Rev. B* **62** 14837 (2000).
- [41] A. K. Murtazaev and A. B. Babaev, *J. Mag. Mag. Mat.* **321** 2630 (2009).
- [42] D. Loison, *Physica A* textbf271(1-2) 157-168 (1999).
- [43] P. Lundow, K. Markström, and A. Rosengren, *Philos. Mag.* **89** 2009 (2009).

- [44] E. Jones, T. Oliphant and P. Peterson, SciPy: Open source scientific tools for Python (2014).
- [45] E. P. Yelsukov, E. V. Voronina, and V. A. Barinov, *J. Magn. Magn. Mater.* **115** 271 (1992).
- [46] F. Stein and M. Palm *Int. J. Mater. Res.* **98**(7) 580-588 (2007).
- [47] C. J. Willmott, S. G. Ackleson, R. E. Davis, J. J. Fedema, K. M. Klink, D. R. Legates and C. M. Rowe, *J. Geophys Res. Oceans* **90**(C5) 8995-9005 (1985).
- [48] H. Greiner, *Math. Comput. Model.* **15**(10) 97-106 (1991).
- [49] D. R. Legates and G. J. McCabe, *Water Resour. Res.* **35**(1), 233-241 (1999).
- [50] R. D. Shull, H. Okamoto and P. A. Beck, *Solid State Commun.* **20**(9) 863-868 (1976).
- [51] J. B. Santos-Filho and J. A. Plascak, *Comp. Phys. Comm.* **182** 1130 (2011).